A Cross Reference Analysis of Adaptive Piezoelectric Actuator Reinforced Slender Airframes for Microsatellite Launch Vehicles

T. A. Fashanu[1], L. M. Adetoro[2], O. S. Asaolu[1] and A. A. Ayorinde[3]
[1]Department of Systems Engineering, University of Lagos, Nigeria
[2]National Agency for Space Research and Development, FCT Abuja, Nigeria
[3]Department of Electrical and Electronics Engineering, University of Lagos, Nigeria
Corresponding Author email: tfashanu@unilag.edu.ng

Abstract

This work develops and simulates the virtual prototype of a conceptual variable modulus airframe for slender microsatellite launch vehicles. To modulate stiffness, piezoelectric transducers are scientifically positioned at the zeros of the derivatives of the slender airframe shape functions. These transducers are actuated by a Proportional Derivative type control law such that the overall system is globally asymptotically stable in the sense of Lyapunov. By considering typical in-flight parameters, the performance of the conceptual synthetic adaptive airframe is studied in comparison with identical airframe that is made of advanced aerospace composites. Simulation results show that for slender beams with aspect ratios; 10, 12 and 15 respectively, the initial amplitudes of vibrations were effectively damped by factors of 85.95%, 3.02% and 6.06% at the instance of piezoelectric reinforcement. At steady states, in the listed order of aspect ratios, the percentage residual amplitudes of the slender beam's oscillations are 1.53%, 48.34% and 46.55%, respectively. In effect, the conceptual adaptive slender airframe demonstrated very good potential for possible utilization on microsatellite launch vehicles.

Keywords: Piezoelectric Effects, Adaptive Slender Airframe, Stiffness Modulation, Microsatellite Launch Vehicle

Definition of Terms and Symbols

$M_p(x,t)$ - total torque produced by piezoelectric actuators

$M_{pi}(x,t)$ - moment exerted on the beam by the i^{th} actuator

E_p - modulus of elasticity of the piezoelectric

E_b - beam modulus of elasticity of the piezoelectric

d_{31} – Piezoelectric constant

l_b , w_b , t_b – length, width and thickness of the beam, respectively.

l_p , w_p , t_p – length, width and thickness of the each piezoelectric transducer, respectively.

n – total number of identical collocated piezoelectric actuator and sensor pairs that are bonded to the beam

$e_{ai}(t)$ - electric potential difference of the i^{th} actuator

$e_{si}(t)$ - voltage induced in the i^{th} sensor

$f(x,t)$ - is the excitation force per unit length acting on the beam in the transverse direction at location x

$w(x,t)$ - transverse deflection of the synthetic adaptive airframe

$w_p(x)$ - transverse deflection of the airframe due to $M_p(x,t)$

$w_d(x,t)$ - transverse deflection of the airframe at point x and time t due to $\delta \boldsymbol{f}(\boldsymbol{t})$

V_{xyx} - velocity vector for center of gravity of the synthetic adaptive airframe

ω_{xyx} - angular velocity vector about the center of gravity of the synthetic adaptive airframe

f_{xyz} - total external force vector

M_{xyz} - total external moment vector

m - total mass

I_{xyx} - inertia tensor of the rigid body

$\xi_i(t)$ - transverse deflection of the synthetic adaptive airframe in terms of generalized coordinates

$\varphi_i(x)$ - transverse deflection of the synthetic adaptive airframe in terms of the normal modes

$V(\xi t, \dot{\xi}\iota)$ - airframe viscous damping matrix

$G(\xi t, \dot{\xi}\iota)$ - stiffness matrix

1.0 INTRODUCTION

Emerging trends in space development and deployment of space-based technologies are strongly motivating the search for advanced composites for aerospace applications. To be precise, intensive search is ongoing for high performance structural materials for satellite and micro-satellite launch vehicles' frames. In such applications, the candidate composites must satisfy certain performance metrics. These include affordability or mission cost effectiveness, optimum strength to mass ratio, minimal structural vibration or optimal toughness. It should also be physically and chemically stable in space environment (Ni *et al*., 2019). These criteria must be met by the structure under static and dynamic loading; during testing, real flight conditions and finally, in space zero gravity environment. This is in addition to satisfying other subsystems requirements such as design for thermal stability, swift and measured response to attitude control signals, as well as ease of communications between the space vehicle and base station, etc., (Cadieu *et al*., 2020; Belbachir *et al*., 2020).

To meet these requirements, aerospace composites are mostly synthetic multiphase light weight solid materials that consist of two or more simple materials. Individually, these components have distinct characteristics and configuration (Draiche et al., 2019). Basically, two types of functionalities are required of the constituents. They either serve as the matrix material or its reinforcement. On the whole, the desired outcome of an effectively formed aerospace composite is high specific strength and high specific modulus (Caminero et al., 2017).

When formed, hybrid materials do not only reserve the merits of their constituents; they also overcome some of their intrinsic defects. In addition, composites could also exhibit excellent capabilities that the basic components do not possess. Therefore, in aerospace applications, advanced composites that use new type isotropic material constituents are evolving. For example, the carbon fiber epoxy resins are the leading unidirectional composites that are widely applied in aerospace structures (Lutjering *et al*., 2007).

Like many modern aerospace vehicles, the need to save weight and cost in order to realize functional light weighted structure on slender launch vehicle has led to tradeoffs between mechanical design, inertia, aspect ratio and stiffness. Hence, the outcome is a body that is quasi rigid and quite susceptible to low frequencies structural vibration modes (Yang *et al*., 2020).

According to Beaumont (2014), operational environment and low frequency vibrations may negatively affect long-term durability of engineering composites that are used for the construction of light weight slender launch vehicle airframes. More recently, additional requirements such as varying mechanical properties are placed on toughened composites to meet airframes specifications. For this purpose, some functionally graded materials (FGM) have been developed to meet these new requirements while

satisfying necessary financial constraints. Consequently, variable stiffness composites are now available for the development of slender microsatellite launchers (Hayward and Urdiales, 2018). However, despite their considerable advantage over conventional composites, the FGMs are also limited by cost and weight. As a result, alternative approaches to composite toughening processes are presently been explored to develop advanced composites with functional weights at affordable cost for aerospace applications (Srinivas *et al*., 2020).

Meanwhile, a class of anisotropic piezoelectric materials exists; their mechanical response differs in different directions under induced electric field (Karley, 1983). These are piezoelectric transducers; they facilitate coupling between electrical and mechanical parameters. When electric field is applied, the piezo-electrics are known to induce mechanical deformation, (Torbati *et al*., 2022). The reverse is also true. On a broader scale, many studies have been conducted on the behavior of composite piezoelectric materials. This is due to their wide areas of applications (Simpson *et al*., 1998; Ludwiczak, 2006; Wu, 2010; Konka, 2011).

Hence, in this work, piezoelectric transducers are explored as electromechanical compensators that can modulate the numerical equivalence of the stiffness matrix of a conceptual airframe in linear elastic stress-strain relations. This would facilitate tradeoffs between structural stiffness, materials' weight, optimum cost and vibration damping on the airframe. For this purpose, transducers are bonded to the flexible structure and utilized as either sensors to monitor deflections; or as actuators, to regulate airframe oscillation. This is the synthetic adaptive airframe. For some rather different applications, some noteworthy contributions to this innovative concept include (Hector *et al.,* 2016), as well as (Zagrai *et al.,* 2010).

In aerospace community, realization of variable modulus airframes based on piezoelectric transducers that are embedded on non-piezoelectric composite material is still a relatively new research concept. It holds promise for the development of modern Launch Vehicle airframes. Summarily, using Matlab Simulink Blocks, this work developed a virtual similitude of a conceptual piezoelectric transducer reinforced slender airframe for micro satellite launch vehicle. Subsequently, the performance of this smart structure is compared with that of advanced composites that are presently available for the construction of aerospace structures.

2.0 GOVERNING DIFFERENTIAL EQUATIONS

To derive the mathematical model of synthetic adaptive airframe, the following assumptions are made:

- Airframe length is much longer than its diameter. It is an Euler Bernoulli beam.
- Perfect bonding exists between the airframe and piezoelectric transducers such that there is no energy loss at the interface of the bond.
- The piezoelectric actuators are strictly located at zeros of the derivative of the shape function
- The induced piezoelectric moment is a point load which acts transversely along the pitch plane
- The equation of motion represents perturbations from a nominal steady state condition.

From the considerations given above, when subjected to electric potential difference, the total mechanical torque produced by piezoelectric actuators is expressed as;

$$M_p(x,t) = \sum_{i=1}^{n} M_{pi}(x,t) \quad (1)$$

For regular piezoelectric transducers, the control moment exerted on the beam by the i^{th} actuator is expressed by Moheimani and Fleming, (2006), as;

$$M_{pi}(x,t) = \left(\frac{E_b E_p t^2{}_b w_b w_p d_{31}}{E_b l_b w_b + E_p t_p w_p}\right) e_{ai}(t) \quad (2)$$

Here E_p is the modulus of elasticity of the piezoelectric. E_b is the beam modulus of elasticity, d_{31} is piezoelectric constant. n is the total number of identical collocated piezoelectric actuator and sensor pairs that are bonded to the beam. The i^{th} actuator is subjected to an electric potential difference $e_{ai}(t)$ and the voltage induced in the i^{th} sensor is $e_{si}(t)$. The beam has length l_b, width w_b, and thickness t_b. Corresponding dimensions of each piezoelectric transducer are l_p, w_p and t_p. $f(x,t)$ is the excitation force per unit length acting on the beam in the transverse direction at location *x,* and piezoelectric actuator is configured to generate moment $M_p(x,t)$ which act opposite to the applied load.

2.1 Virtual Prototyping and Implementation Framework

To configure a virtual test rig for performance analysis of the conceptual piezoelectric actuated airframe, we consider a (slender) Euler Bernoulli beam that is bonded with transducers at strategic locations as shown in Figure 1. The Figure further illustrates the positions of the transducers relative to the beam's mode shape and how the studied beam is applied on a slender launch vehicle.

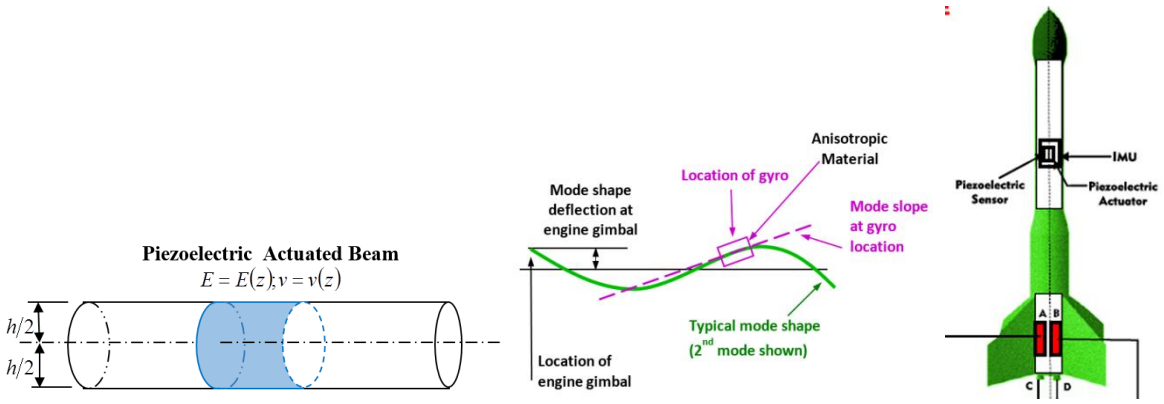


Figure 1: Slender Euler Bernoulli Beam Strategically Bonded with Piezoelectric Transducers

2.2 Vibration Equation of Synthetic Adaptive Airframe

The deflection dynamics of the smart electromechanically reinforced airframe with finite number of (bonded) piezoelectric transducers is presented as an Euler Bernoulli's beam under a free – free boundary condition such that;

$$\rho A\frac{\partial^2 w}{\partial t^2}+EI\frac{\partial^4 w}{\partial x^4}=M_p(x,t)+f(t)\delta \tag{3}$$

subject to the following boundary conditions;

$$w|_{t=0}=w(x,0),\frac{\partial w}{\partial t}\bigg|_{t=0}=\dot{w}(x,0);$$
$$EI\frac{\partial^2 w}{\partial x^2}\bigg|_{\substack{x=0\\x=l}}=0,\left(EI\frac{\partial^3 w}{\partial x^3}\right)\bigg|_{\substack{x=0\\x=l}}=0. \tag{4}$$

Using the method of separation of variables, the transverse deflection $w(x,t)$ of the synthetic adaptive airframe in terms of generalized coordinates $\xi_i(t)$ and the normal modes $\phi_i(x)$ can be expressed as;

$$w(x,t)=\sum_{i=1}^{\infty}\phi_i(x)\xi_i(t) \tag{5}$$

Given the conditions stated in Equation (4), solution of Equation (3) as normalized mode shapes $\phi_i(x)$ admit the representation in Equation (6), (Lanre et al., (2014));

$$\phi_i(x)=\left[\left[\cosh(\lambda_i x)+\cos(\lambda_i x)\right]-\frac{\sinh(\lambda_i L)+\sin(\lambda_i L)}{\cosh(\lambda_i L)-\cos(\lambda_i L)}\left[\sinh(\lambda_i x)+\sin(\lambda_i x\right]\right] \tag{6}$$

Where, $\lambda_1 L=4.730;\lambda_2 L=7.853;\lambda_3 L=10.996;\lambda_4 L=14.137$ for free beams and the constants λ_i are the Eigen-values of the modal shape function $\phi_i(x)$ in Equation (5).

Taking into account the piezoelectric induced effect with variations in stiffness properties in different directions, the superposition of $w_p(x)$ and $w_b(x,t)$ is computed for Equation (5) by expressing $w(x,t)$ as,

$$w(x,t)=w_p(x)+w_d(x,t) \tag{7}$$

Here $w_d(x,t)$ is the transverse deflection of the airframe at point *x* and time *t* due to $f(t)\delta$ and $w_p(x)$ is transverse deflection of the airframe due to $M_p(x,t)$.

Substituting Equation (7) into Equation (3) yields;

$$b_b\rho_b t_b\frac{\partial^2 w_b(x,t)}{\partial t^2}+b_p\rho_p t_p\frac{\partial^2 w_b(x,t)}{\partial t^2}+E_bI_b\frac{\partial^4 w_b(x,t)}{\partial x^4}+E_pI_p\frac{\partial^4 w_p(x)}{\partial x^4}=M_p(x,t)+f(t)\delta \tag{8}$$

Consequent upon which the mechanical and electrical components of Equation (8) are established as;

$$b_b\rho_b t_b\frac{\partial^2 w_b(x,t)}{\partial t^2}+E_bI_b\frac{\partial^4 w_b(x,t)}{\partial x^4}=f(t)\delta \tag{9}$$

$$b_p\rho_p t_p\frac{\partial^2 w_p(x,t)}{\partial t^2}+E_pI_p\frac{\partial^4 w_p(x)}{\partial x^4}=M_p(x,t) \tag{10}$$

Equations (9) and (10) define the electromechanical coupling of the dynamics of the piezoelectric reinforced adaptive airframe. To proceed, we compute the composite dynamic response of the electromechanical equivalence of the adaptive airframe. This is addressed in Section 2.3.

2.3 Deflections Dynamics of Piezoelectric Actuated Adaptive Airframe

As indicated earlier, the deflection of the adaptive airframe $w(x,t)$ is the sum of its mechanical $w_d(x,t)$ and electrical $w_p(x,t)$ response such that;

$$w(x,t) = w_p(x,t) + w_d(x,t) = \sum_{i=1}^{\infty} \phi_i(x)\xi_i(t) \tag{11}$$

However, according to Equation (5), differentiating under the sign, we can write;

$$\frac{\partial^4 \left(w_p(x,t) + w_d(x,t)\right)}{\partial x^4} = \sum_{i=1}^{\infty} \frac{\partial^4 \phi(x,t)}{\partial x^4} \xi(t) \tag{12}$$

$$\frac{\partial^2 \left(w_p(x,t) + w_d(x,t)\right)}{\partial t^2} = \sum_{i=1}^{\infty} \frac{\partial^2 \xi(x,t)}{\partial t^2} \phi(x) \tag{13}$$

Considering a mass-spring-damper type deflection dynamics, the general coordinate $\xi_i(t)$ of the airframe can be presented as:

$$\ddot{\xi}_i(t) + \omega_i^2 \xi_i(t) = p(x,t) \tag{14}$$

where $$p(x,t) = \frac{2}{\rho_p A_p} \int_0^L M_p(x,t)\phi(x)dx + \frac{2}{\rho_b A_b} \int_0^L f(t)\delta(x-a)\phi(x)dx \tag{15}$$

2.4 Rigid Body Dynamics of Synthetic Adaptive Airframe

To complement the developments in Sections 2.2 and 2.3; in 3-Dimensional vector notations, the dynamics of an airframe can be described by the system of non-linear differential equations as;

$$\frac{dv_{xyz}}{dt} = \frac{f_{xyz}}{m} - \omega_{xyx} \times v_{xyx} \tag{16}$$

$$\frac{d\omega_{xyz}}{dt} = I_{xyz}^{-1}\left(M_{xyz} - \omega_{xyz}\right) \times \left(I_{xyx} \times \omega_{xyx}\right) \tag{17}$$

where v_{xyx} is velocity vector for center of gravity (c.g.). c.g. represents rigid body centre of mass, ω_{xyx} is angular velocity vector about the c.g. f_{xyz} is total external force vector, M_{xyz} is total external moment vector, m is total mass, I_{xyx} is inertia tensor of the rigid body.

2.5 Parameters Identification of Bending Modes and Rigid Body Dynamics

Letting the deflection $\boldsymbol{x}_1 = \xi_i$ and deflection rate $\boldsymbol{x}_2 = \dot{\xi}_i$; in state space form, the rigid-bending mode (i.e., quasi rigid) dynamics of the synthetic adaptive airframe can be represented as:

$$\begin{bmatrix} \dot{\boldsymbol{x}}_1 = \boldsymbol{x}_2 \\ \dot{\boldsymbol{x}}_2 = -\omega_i \boldsymbol{x}_1 + \boldsymbol{p(x,t)} \end{bmatrix} \tag{18}$$

such that rigid body –bending mode equilibrium of adaptive airframe i.e. $\dot{\boldsymbol{x}}_1 = \dot{\boldsymbol{x}}_2 = 0$ becomes;

$$\begin{bmatrix} 0 = \boldsymbol{x}_2 \\ 0 = -\omega_i \boldsymbol{x}_1 + \boldsymbol{p(x,t)} \end{bmatrix} \tag{19}$$

from which, $\xi_i(\boldsymbol{t}) = \dfrac{\boldsymbol{p(x,t)}}{\omega_i}$ and $\dot{\xi}_i = 0$. (20)

Then solution of the generalized coordinates $\xi_i(\boldsymbol{t})$ in Equation (20) established the relationship between bending fatigue at low bending mode frequency ω_i and the excitation force per unit length. This solution was presented by Palacios et al., (2010).

2.6 Non-piezoelectric Composite Beam Vs Piezoelectric Actuated Composite Beam

Without the adaptive piezoelectric effect, $\boldsymbol{p(x,t)} = \boldsymbol{f(x,t)}$ corresponds to non-piezoelectric composite beam with natural frequencies ω_i , such that;

$$\xi_i(\boldsymbol{t}) = \frac{\boldsymbol{f(x,t)}}{\omega_i} \tag{21}$$

Therefore, for a (regular) Euler Bernoulli Beam, $\xi_i(\boldsymbol{t}) = 0$ if $\boldsymbol{f(x,t)} = 0$ or that ω_1 is at high frequencies. However, for piezoelectric composite beam, $\xi_i(\boldsymbol{t}) = 0$ if $\boldsymbol{M_p(x,t)} = \boldsymbol{f(x,t)}$ or ω_1 is at high frequencies. Consequently, the dynamic equilibrium conditions of $\boldsymbol{M_p(x,t)} = \boldsymbol{f(x,t)}$ can be used to regulate the numerical equivalence of stiffness matrix in linear elastic stress-strain relations at low bending mode frequencies.

Hence, for the design of the proposed smart structure, the outlined matching condition is quite important. It provides the basis for adapting piezoelectric energy from piezoelectric transducers to dampen oscillations resulting from airframe slenderness. Thus, trading off weight to significantly improve the performance of piezoelectric composite beam beyond the limits of conventional aerospace composite beam. This is the theoretical background of the innovative concept of deploying piezoelectric actuated forces on Euler Bernoulli airframe to attenuate deflections.

3.0 EMBEDDING PIEZOELECTRIC EFFECTS ON COMPOSITE AIRFRAME

The effect of $M_p(x,t)$ loading on the dynamics of the composite Euler Bernoulli beam can be included quite simply by setting $M_p(x,t) = f(x,t)$, where $M_p(x,t)$ has the magnitude of the external loading but acts in the opposite direction.

This is equivalent to airframe oscillating upward with acceleration $\ddot{\xi}_i(t)$. This upward acceleration causes exactly the same effect on the airframe as piezoelectric actuator would oscillate in virtual downward direction. So, with no additional computational cost, the stiffness required for structural stability at all frequencies is induced without increasing the weight (i.e. thickness) of the slender airframe.

4.0 IMPLEMENTATION OF PIEZOELECTRIC STIFFNESS REGULATOR ON SLENDER AIRFRAME

In order to study the variable stiffness properties of synthetic adaptive airframe such that $\xi_i(t) = 0$ at the location of piezoelectric transducers. We consider the airframe with dynamics given by;

$$M_p(\xi_i,t) = f(\xi_i,t) = M(\xi_i)\ddot{\xi}_i + V(\xi_i,\dot{\xi}_i) + G(\xi_i) \tag{22}$$

In terms of the young modulus $\xi_i \Rightarrow \pm\xi_i(E_b)$, the Proportional Derivative PD actuator's control law is expressible as;

$$M_p(\xi_i,t) = \pm\left(K_p E(\xi_i) + K_d\dot{\xi}_\iota\right) + G(\xi_i) \tag{23}$$

in which K_p and K_d are positive definite matrices, $M(\xi_i)$ is mass matrix, $V(\xi_i,\dot{\xi}_i)$ is airframe viscous damping matrix and $G(\xi_i)$ is the stiffness matrix. Following the mode shape function, the $\pm$ sign on the right-hand side of Equation (23) accounts for the alternating positions of the beam's deflection with respect to its center line.

The resulting closed-loop system obtained by equating Equations (22) and (23) is given as;

$$M(\xi_i)\ddot{\xi}_i + V(\xi_i,\dot{\xi}_i) + K_d\dot{\xi}_i = K_p E \tag{24}$$

To guarantee global asymptotic stability of Equation (24), Chen et al, (2006) suggests a candidate quadratic Lyapunov function of the form,

$$V(M(\xi_i),\dot{\xi}_i,E(\xi_i)) = \frac{1}{2}\dot{\xi}_i^T M(\xi_i)\dot{\xi}_i + \frac{1}{2}E^T K_p E \tag{25}$$

Clearly, Equation (25) is positive definite everywhere or zero at the origin. This is guaranteed, because the mass matrix, M (ξ_i), and the gain matrix, K_p, are positive definite matrices.

Differentiating (25) along the direction of the system's dynamics yields;

$$\begin{aligned}\dot{V} &= \frac{1}{2}\dot{\xi}_i^T\dot{M}(\dot{\xi}_i)\dot{\xi}_i + \dot{\xi}_i^T M(\xi_i)\ddot{\xi}_i - E^T K_P\dot{\xi}_i \\ &= \frac{1}{2}\dot{\xi}_i^T\dot{M}(\xi_i)\dot{\xi}_i - \dot{\xi}_i^T K_d\dot{\xi}_i - \dot{\xi}_i^T V(\xi_i,\dot{\xi}_i) \\ &= -\dot{\xi}_i^T K_d\dot{\xi}_i\end{aligned} \tag{26}$$

Meanwhile, the electro mechanical relations derived from Equation (22) are; $\dot{\xi}_i^T \boldsymbol{M}(\xi_i)\ddot{\xi}_i = -\dot{\xi}_i^T \boldsymbol{K}_d \dot{\xi}_i$; $\boldsymbol{E}^T \boldsymbol{K}_P \dot{\xi}_i = \dot{\xi}_i^T \boldsymbol{V}(\xi_i, \dot{\xi}_i)$. Consequently, given that K_d is positive definite. Equation (26) is negative definite. In taking the last step in (26), we have made use of interesting matching conditions stated in Equation (27); i.e.,

$$\boldsymbol{M}_p(x,t) = \boldsymbol{f}(x,t) \text{ or } \boldsymbol{w}_p(x,t) = -\boldsymbol{w}_d(x,t) \quad (27)$$

which dictates that,

$$\frac{1}{2}\dot{\xi}_i^T \dot{\boldsymbol{M}}(\xi)\dot{\xi}_i = \xi_i^T \boldsymbol{V}(\xi_i, \dot{\xi}_i) \quad (28)$$

Thus, in view of Equation (26) and its consequent electromechanical relationships, the control law in Equation (23) as applied to the system in Equation (22) would achieve global asymptotic stability.

Hence, by regrouping Equation (14) in line with Equations (22) and (23); Equation (24) with feedback loop is configured so that the airframe is adaptive and that its origin (i.e., the fixed points $\xi_i = 0, \dot{\xi}_i = 0$) of the piezoelectric actuated slender airframe is globally asymptotically stable in real time.

4.0 SIMULINK FRAMEWORK FOR ADAPTIVE AIRFRAME SIMULATION AND TESTING

The Simulink Scheme in Figure 2 is advanced to test and simulate the dynamics of the variable modulus slender airframe. The objective is to virtually prototype and prove the conceptual smart airframe for possible application on microsatellite launch vehicles.

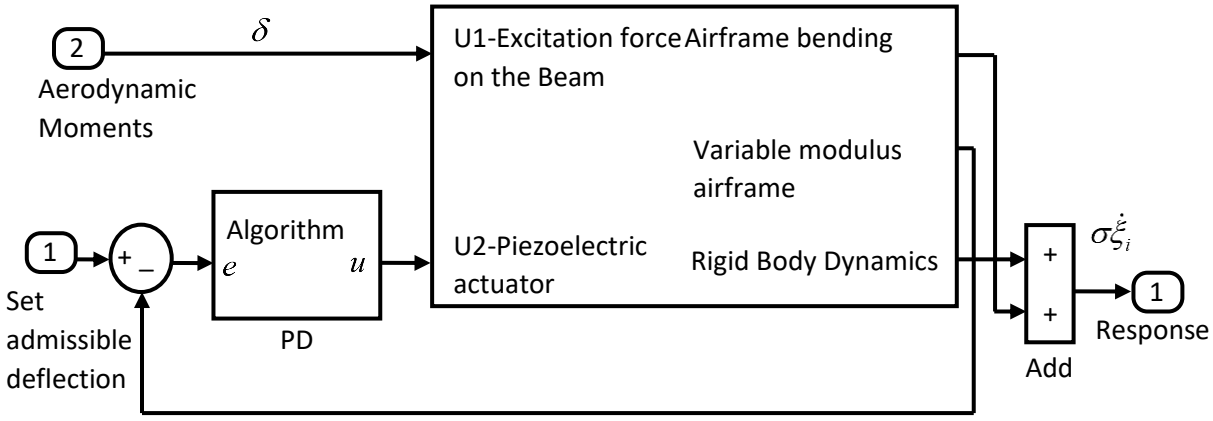


Figure 2: Simulink Blocks for Simulating the Response of Synthetic Adaptive Airframe

4.1 Instrumentation and Adaptive Control of Piezoelectric Actuated Slender Airframe Bending Mode

The simulation in Figure 2 is developed to realize a model-based real time controller that can effectively damp fluttering oscillations, and regulate bending modes on slender airframes via the use of piezoelectric actuators and sensors. As established earlier, this regulator is constrained to follows a Lyapunov typed Proportional Derivative (PD) control law. The virtual form of the controller is implemented on Matlab-Simulink platform.

The coupled systems rearrangement for active smart airframe prototyping admits the representation shown in Figure 3.

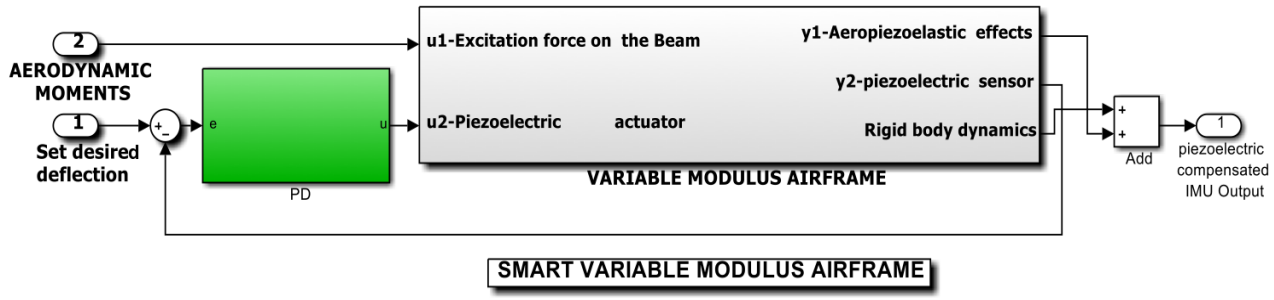


Figure 3: Active Simulink Block for Response Analysis of Slender Adaptive Airframe

In addition to Figures 2 and 3; Table 1 presents the simulation parameters for comparative analysis of the dynamic response of a synthetic composite airframe and the conceptual piezoelectric actuated adaptive airframe.

Table 1: Dimensions and Properties of Composite Airframe and Adaptive Piezoelectric Airframe

Slender Airframe Type	Parameter	Value
Synthetic Conventional Airframe	Length L_b	30m
	Width w_b	3m
	Thickness t_b	3mm
	Density ρ_b	2.77 x10^3 Kg/m^3
	Young Modulus $\boldsymbol{E_b, E_p}$	7x10^{10}N/m^2,6.3x10^{10}N/m^2
Piezoelectric (PIC255) Reinforced Adaptive Airframe	Length $\boldsymbol{L_p}$	50mm each
	Width $\boldsymbol{w_p}$	25mm
	Thickness $\boldsymbol{t_p}$	0.25mm
	Piezoelectric Constant $\boldsymbol{d_{31}}$	11.2Cm^2
	Charge Constant e_{33}	-210x10^{-12}m/V
	Capacitance	115nF

Adapted from: Lanre et al. (2014).

The Simulink Blocks study the responses of synthetic adaptive airframe and that of conventional launch vehicle airframe at different (geometrical) aspect ratios and bending mode frequencies.

5.0 SIMULATION RESULTS

Considering a proportional derivative PD control law of the type $\boldsymbol{M_p(x,t) = 9.6s + 27}$, with initial launch load distribution of the form $F(x) = -0.05x \quad 0 \le x \le 30m$, and subject to an initial deflection velocity $\dot{w}_0(x,0) = 0$, and initial deflection $w_0(x,0) = 0.002$ m at each point on the airframe. The dynamic

response of the deflections of the slender airframe, and piezoelectric actuated slender airframes is studied for spectral characteristics of 7.491Hz, 6.047Hz given that the structure is airborne at 4.043Hz.

The corresponding aspect ratios of the airframes studied are 10, 12, and 15. Results obtained are presented in the curves shown in Figures 4 to 8.

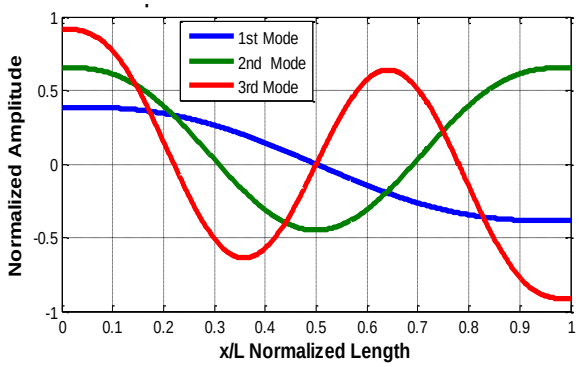
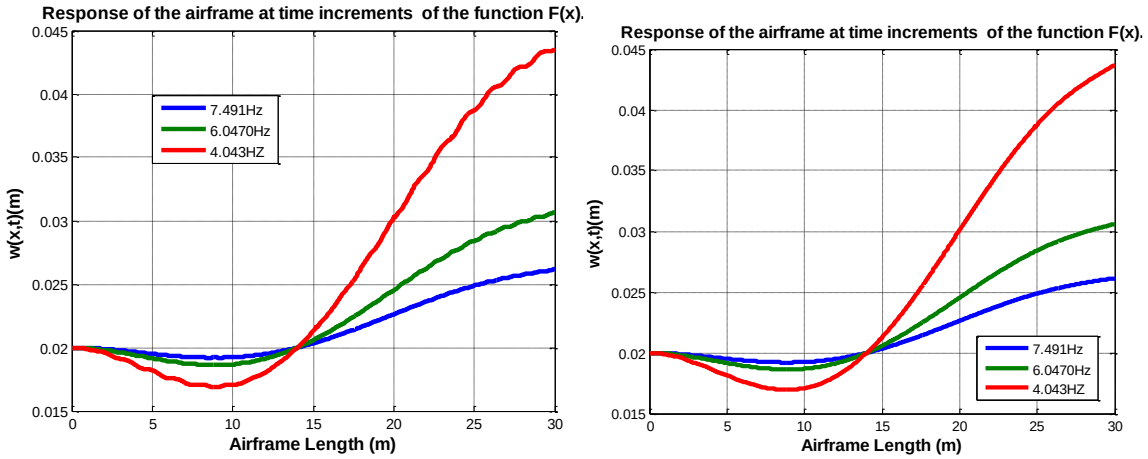


Figure 4: Slope of Slender Airframe in Free Vibration (F(x) = 0)



(a) (b)

Figure 5: (a) Response of slender airframe to F(x) (b) Response of synthetic adaptive slender airframe to F(x)

Figure 5 compares responses for a slender airframe and synthetic adaptive slender airframe in this study. Comparison of results shows that the concept of embedding smart material technology on non-piezoelectric composite beam eliminate the effects of structural oscillation on slender airframe.

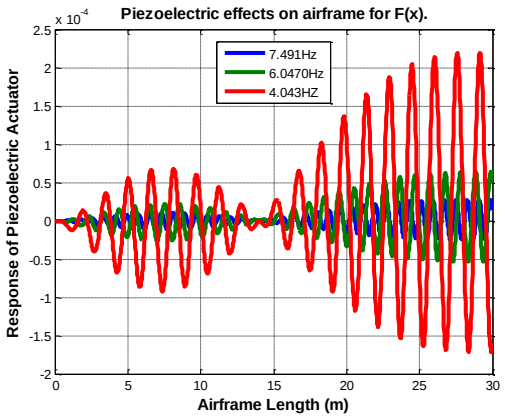
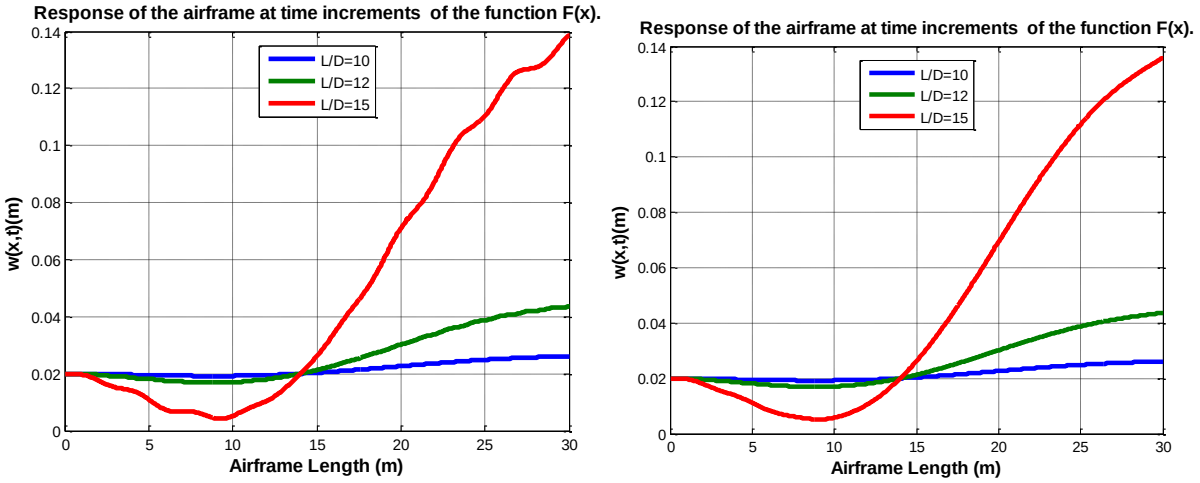


Figure 6: Energy Dissipation Rate on Synthetic Adaptive Airframe

Oscillation damping abilities of the piezoelectric actuators are characterized for three test frequencies, namely 4.043Hz, 6.047Hz and 7.491Hz, respectively, and illustrated in Figures 5 and 6. The piezoelectric damping actuator effectively damped out the 4.043Hz oscillation and its performance follows according to the order of magnitudes of the natural frequency of the oscillation. Furthermore, the energy dissipation capability of the piezoelectric transducers and consequent realization of the variable modulus airframe configuration is indicated in Figure 6. It is shown that the magnitude of piezoelectric actuator damping energy is highest at 4.043Hz and lowest for the 7.491Hz spectral characteristics.



(a) (b)

Figure 7: (a) Response of slender airframe to F(x) (b) Response of synthetic adaptive airframe to F(x).

Considering a composite airframe with young modulus $7x10^{10}N/m^2$ subjected to step input at 6.0469Hz. Figure 7 presents the influence of F(x) across the airframe for various values of aspect ratios, namely 10, 12 and 15, respectively. The first bending mode of the slender airframe oscillates with a reference overshoot of 46.38% at a peak time of 2.9501sec. However, to illustrate the efficacy of the piezoelectric controlled adaptive airframe, the gains of the PD control law were tuned to K_p=27 and K_d =9.6, respectively.

As shown in Figure 7b, oscillations damping effect of the actuators on the first and second bending modes increased. It reduced the percentage overshoot from 46.549% to 6.063%, and from 48.38% to 3.015%, respectively, after 10s. Thus, the piezoelectric actuator damping rate increases with aspect ratio.

An illustration of the rate of energy dissipation of piezoelectric transducers on the synthetic adaptive airframe is shown in Figure 8. Here, the rate increases with aspect ratio. Similarly, the corresponding numerical values and relative performance of the smart variable modulus airframe of Figure 7 at aspect ratios of 10, 12 and 15 are evaluated in Table 2.

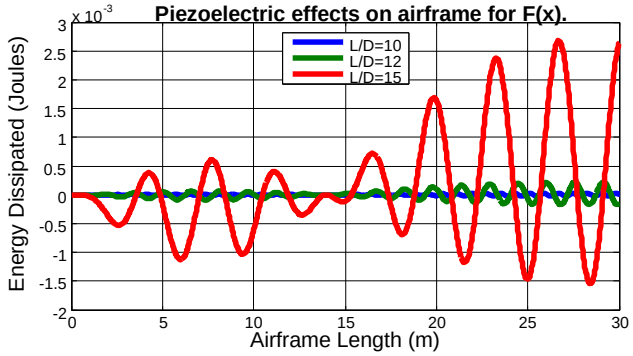


Figure 8: Energy Dissipation Profile on Synthetic Adaptive Airframe in Response to F(x)

Table 2: Performance of Smart Variable Modulus Airframe @ 10, 12 and 15 Aspect Ratios.

Aspect ratio	Bending mode frequency (rad/sec)	Peak amplitude before piezoelectric effects	Initial amplitude at instant of piezoelectric effects	Initial % peak amplitude reduction	Final amplitude reduction	Final %peak amplitude reduction
15	1.824	0.2111	0.1983	6.0637%	0.01059	46.549%
12	4.043	0.0567	0.04272	3.015%	0.00324	48.34%
10	7.941	0.01647	0.002317	85.95%	0.001242	1.53%

Considering a slender airframe with Young Modulus $7x10^{10}N/m^2$ subjected to step input at 6.0469Hz as indicated in Table 2. Simulation outcomes show that the first bending modes of the synthetic adaptive airframe oscillate with a reference overshoot of 46.38% at a peak time of 2.9501sec. However, using a Lyapunov based PD control law with K_p=27 and K_d=9.6; oscillations of the first and second bending modes are damped such that the percentage overshoot decreased from 46.38% to 6.063% and from 48.34% overshoot to 3.015%, respectively, after 10s.

6.0 CONCLUSION

In order to address the growing demand for efficient and responsive microsatellite Launch Vehicles, this work developed a real-time innovative and compact solution for bending modes stabilization on slender airframes. The transient time response analyses of electromechanical stabilized airframe that uses an actuator to modulate its stiffness matrix in linear elastic stress-strain relations at low bending mode frequencies are achievable by integrating piezoelectric transducers on conventional airframes. Thus, piezoelectric energy from piezoelectric transducers can be used to trade off weight, and support slenderness at low cost to improve mission performance and affordability of synthetic adaptive

airframes for microsatellite launch vehicles, when compared with other advanced aerospace composite beams.

REFERENCES

Adelfang, S. I., & Smith, O. E. (1998). Gust models for launch vehicle ascent. *In 36th AIAA aerospace sciences meeting and exhibit,* pp. 1-8.

Belbachir N., Bourada M., and Draiche K. (2020). Thermal flexural analysis of anti-symmetric cross-ply laminated plates using a four variable refined theory," *Smart Structures and Systems*, 25(4) 409–422,

Beaumont, P. W. (2014). On the problems of cracking and the question of structural integrity of engineering composite materials. *Applied Composite Materials,* 21(1) 5-43.

Bolender, M. A., & Doman, D. B. (2005). A non-linear model for the longitudinal dynamics of a hypersonic air-breathing vehicle. *AIAA paper*, 6255, 2005.

Braun, R. D., Putnam, Z. R., Steinfeldt, B. A., & Grant, M. J. (2013). Advances in inertial guidance technology for aerospace systems. *In AIAA Guid-ance, Navigation, and Control Conference. Boston: AIAA,* pp. 1-18.

Cadieu L, Kopp J. B., and Jumel J. (2020). Temperature effect on the mechanical properties and damage mechanisms of a glass/thermoplastic laminate. *J Composite Matls*, Vol.54 (17), 2271–2282. Caminero M. A., García-Moreno I., and Rodriguez G. P. (2017). Damage resistance of carbon fibre reinforced epoxy laminates subjected to low velocity impact: effects of laminate thickness and ply- stacking sequence. *Polymer Testing*, 63, 530–541.

Chen, C. W., Chiang, W. L., Tsai, C. H., Chen, C. Y., & Wang, M. H. (2006). Fuzzy Lyapunov method for stability conditions of nonlinear systems. *International Journal on Artificial Intelligence Tools*, *15*(02), 163-171.

Draiche K., Bousahla A. A., and Tounsi A. (2019). Static analysis of laminated reinforced composite plates using a simple first-order shear deformation theory. *Computers and Concrete*, 24(4), 369–378,

Farris, T. N., Szolwinski, M. P., & Harish, G. (2000). Fretting in aerospace structures and materials. In Fretting Fatigue: Current Technology and Practices. ASTM International.

Fouquart, Y., & Bonnel, B. (1980). Computations of solar heating of the earth's atmosphere- A new parameterization. Beitraegezur Physikder Atmosphaere, 53, 35-62.

Hall, R. M., Holland, S. D., & Blevins, J. A. (2011). Aerodynamic Characterization of a Modern Launch Vehicle. *AIAA Paper*, 10, 2011.

Hayward, K., & Urdiales J. M., (2018). Small Satellite Launch Vehicle from a Balloon Platform. *Proceedings of the 13th Reinventing Space Conference,* 177-192.

Hector, M., Scott, A.R., Victor, E.B., & Anne, C. G, (2016). Mechanical and electromechanical response of LiCo02 cathode using reconstructed microstructures. *Electrochemical Acta*, 190, 1- 15

Johansen, T. A., Shorten, R., & Murray-Smith, R. (2000). On the interpretation and identification of dynamic Takagi-Sugeno fuzzy models. *IEEE Transactions on Fuzzy systems*, 8(3), 297-313.

Karley, L. J. (1983). U.S. Patent No. 4,400,642. Washington, DC: U.S. Patent and Trademark Office.

Lakes, R. (1987). Foam structures with a negative Poisson's ratio. *Science*, 235, 1038-1041.

Lanre A. M., Fashanu T. A., and Osheku C. A. (2014). Parameterization of Micro Satellite Launch Vehicle. *Journal of Aeronautics and Aerospace Engineering*, 3(2), 8-21

Lutjering, G., &Williams, J. C. (2007). Engineering Materials and Processes.

Moheimani, S.O.R and Fleming J. Andrew (2006). Advances in Industrial Control. Copyright by Springer-Verlag London Limited.

Moser, W., Antes, H., & Beer, G. (2005). Soil-structure interaction and wave propagation problems in 2D by a Duhamel integral based approach and the convolution quadrature method. *Computational Mechanics*, 36(6), 431-443.

Ni N., Bian K., and Lu X. I. (2019). Application of advanced composite materials for UAV. *Journal of Aeronautical Materials*, 39(5) 45–60.

Palacios, R., Murua, J., & Cook, R. (2010). Structural and aerodynamic models in nonlinear flight dynamics of very flexible aircraft. *AIAA journal*, *48*(11) 2648.

Srinivas, A. M., Talukder A., Yufeng, Z., Williams, J.C., & Rajarshi, B. (2020). Influence of post deposition annealing on microstructure and properties of laser additively manufactured titanium copper alloys. *Additive manufacturing*, 32, 101067

Straub, J. (2012, May). Cubesats: A low-cost, very high-return space technology. *In Proceedings of the 2012 Reinventing Space Conference.*

Sutton, G. P., & Biblarz, O. (2017). Rocket propulsion elements. John Wiley & Sons.

Tenney, D. R., Davis Jr, J. G., Pipes, R. B., & Johnston, N. (2009). NASA composite materials development: lessons learned and future challenges.

Torbati, M., Davis Jr, Mozaffari, K., Liu, L &Sharma, P, N. (2022). Coupling of mechanical deformation and electromagnetic fields in biological cells, *Rev. Mod. Phys*. 94(2) 61.

Yang, X., Wang C., & Lai, S.K. (2020). A magnetic levitation-based tristable hybrid energy harvester for scavenging energy from low-frequency structural vibration. *Engineering Structures*, 221, 0141-0296.

Zagrai A., Doyle, D., Gigineishvili, V., Brown, J., Gardenier, H., & Arritt, B (2010). Piezoelectric Wafer Active Sensor Structural Health Monitoring of Space Structures. *Journal of Intelligent Material Systems and Structures*, Vol. 21(9), 921-940.

Zhang W., Meng G., Li H. (2006). Adaptive vibration control of micro-cantilever beam with piezoelectric actuator in MEMS. *J Advance Manufacturing Technology*, 321-327.

Zolghadri, A. (2012). Advanced model-based FDIR techniques for aerospace systems: Today challenges and opportunities. *Progress in Aerospace Sciences*, 53, 18-29.